Effect of Gd on the microstructure of as-cast Mg-4.2Zn-0.8Y (at.%) alloys

Wu, J.; Chiu, Y.l.; Jones, I.p.

DOI:
10.1016/j.jallcom.2015.11.209

Document Version
Peer reviewed version

Citation for published version (Harvard):
Wu, J, Chiu, YL & Jones, IP 2016, 'Effect of Gd on the microstructure of as-cast Mg-4.2Zn-0.8Y (at.%) alloys', *Journal of Alloys and Compounds*, vol. 661, pp. 455-460. https://doi.org/10.1016/j.jallcom.2015.11.209

Accepted Manuscript

Effect of Gd on the microstructure of as-cast Mg-4.2Zn-0.8Y (at. %) alloys

J. Wu, Y.L. Chiu, I.P. Jones

PII: S0925-8388(15)31765-5

DOI: 10.1016/j.jallcom.2015.11.209

Reference: JALCOM 36064

To appear in: *Journal of Alloys and Compounds*

Received Date: 8 June 2015

Revised Date: 25 November 2015

Accepted Date: 27 November 2015

Please cite this article as: J. Wu, Y.L. Chiu, I.P. Jones, Effect of Gd on the microstructure of as-cast Mg-4.2Zn-0.8Y (at. %) alloys, *Journal of Alloys and Compounds* (2016), doi: 10.1016/j.jallcom.2015.11.209.

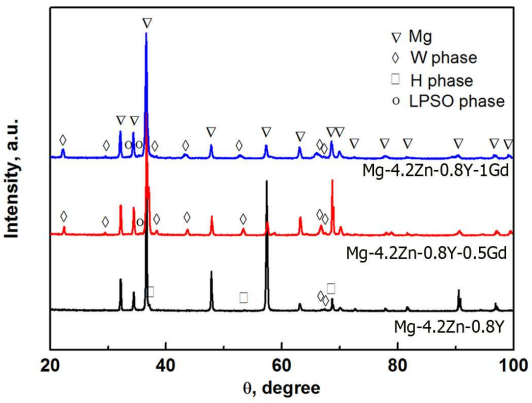

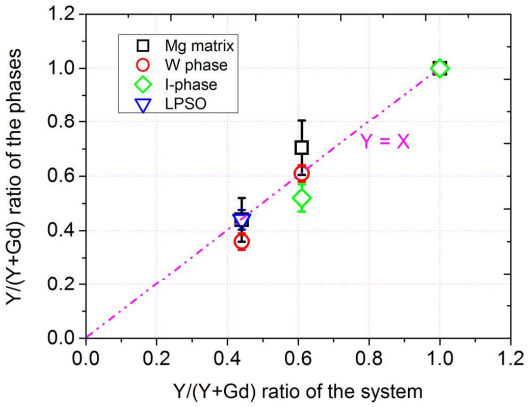

Effect of Gd on the microstructure of as-cast Mg-4.2Zn-0.8Y (at. %) alloys

J. Wu, Y.L. Chiu, I.P. Jones

School of Metallurgy and Materials, University of Birmingham, Edgbaston, Birmingham, B15 2TT, UK

Abstract

The microstructure and hardness of as-cast Mg-4.2Zn-0.8Y-xGd (at. %, x=0, 0.5, 1) alloys were investigated. It has been found that $MgZn_3Y$ (H phase) and $Mg_3Zn_3Y_2$ (W phase) are the main precipitates in the as-cast alloy without Gd. A long-period stacking ordered (LPSO) phase formed upon adding Gd, indicating that the Gd addition enhanced the stability of the LPSO phase. The Gd addition also increased the overall amount of the alloying elements; thus the grain size decreased and the volume fraction of the secondary phases increased resulting in increased hardness of the as-cast alloys. The Y and Gd partition between different phases was investigated. The results show no clear preference between Y and Gd when forming the matrix and the secondary phases, though small fluctuations exist.

Keywords: Magnesium alloys; Gadolinium addition; Long period stacking ordered (LPSO) phase; Quasi-crystalline phase.

1. Introduction

Due to the increasing demands on light materials in the automotive and aerospace industries, more efforts have been devoted to developing Mg alloys in order to obtain competitive or better mechanical properties than those of Al alloys. In recent years, an icosahedral quasi-crystalline phase (i-phase) was found in Mg-Zn-Y alloys (e.g. Mg-4.3Zn-0.7Y at. %) [1]. Due to the high hardness and thermodynamic stability of the i-phase, the alloy exhibited a promising yield strength of ~410 MPa at room temperature [2-4]. By changing the Zn/Y ratio, a Mg-1Zn-2Y at. % alloy was prepared using a powder metallurgy route and the

yield strength of the alloy containing a long-period stacking ordered (LPSO) phase and nano-sized grains was further improved to 610 MPa [5]. Even via casting route, the LPSO-containing Mg-Zn-Y alloys still exhibit a typical yield strength of 270-420 MPa [6-8]. The i-phase and LPSO phase greatly strengthened the Mg. Previous studies [9-15] have shown that the Zn to Y ratio plays a key role in the secondary phase stability in Mg-Zn-Y ternary alloys. With increasing Zn/Y ratio, the stability of the secondary phase increases in the sequence: β ($Mg_{24}Y_5$) → LPSO (18R: $Mg_{10}ZnY$, 14H: $Mg_{12}ZnY$) → W ($Mg_3Zn_3Y_2$) → i-phase (Mg_3Zn_6Y) → Mg_7Zn_3. When Y is replaced by other RE elements, such as Gd, Dy or Ho, although the general trend in ternary phase formation remains similar, the morphology and formation conditions of the secondary phases may differ [16-18]. For example, the LPSO phase of blocky shape forms preferentially along grain boundaries in as-cast Mg-Zn-Y alloys, while in Mg-Zn-Gd alloys the LPSO phase forms as thin lamellae after high temperature aging [18, 19]. Some researchers have focused on the microstructural change in Mg-Zn-Y alloys when Y is partly replaced by Gd. Yang et al. [20] studied Mg-3.9Zn-0.6RE at. % alloys with constant total RE (i.e. Gd and Y) content but varying Gd/Y ratio. They found that increasing the Gd/Y ratio has led to a greater variety of secondary phases present in the alloy. Shi et al. [21] studied Mg-3Zn-3RE at. % alloys with different amount of Y and Gd. They showed that with increasing amount of Gd, the volume fraction of LPSO phase first increased and then decreased. However, the role of Gd on the secondary phase formation still remains unclear. In this paper, the effect of Gd on the microstructure and hardness of Mg-Zn-Y-(Gd) alloys has been investigated. The Y and Gd distributions between the different phases of the alloys, including the Mg matrix, the W phase, the LPSO phase and the i-phase, were also compared. The effect of Gd addition on second phase formation is discussed in light of the results obtained.

2. Experimental procedure

Alloys with a nominal composition of Mg-4.2Zn-0.8Y-xGd (at.%, x=0, 0.5, 1) were prepared using Mg (99.9 wt.%), Zn (99.99 wt.%) and Mg-30Y (wt.%) and Mg-30Gd (wt.%) master alloys. The raw materials were melted and cast in a vacuum induction furnace. Before the melting, the furnace chamber was

pumped down to 4×10^{-1} Torr using a rotary pump and then back filled with Ar gas to 400 Torr. This pumping and re-filling was repeated 3 times. The alloys were then melted in a steel crucible under 400 Torr Ar protection. The melt was held for 10 min and then cast into a 5 mm thick steel mould of 100 mm (length) × 67 mm (width) × 34 mm (height). The mould was located on top of a steel cylinder, also accommodated in the same chamber. The cast alloys were allowed to cool down in the chamber under Ar protection.

The as-cast specimens were examined using a PHILIPS X' Pert X-ray diffractometer (XRD) with a scanning speed of 2°/min and a scanning angle ranging from 20° to 100°. The XRD data was then analysed using MATCH! software with the Crystallography Open Database. The LPSO phase was indexed using crystallographic data from Zhu et al. [14]. The microstructures of the as-cast alloys were characterized using a ZEISS Axioskop 2 optical microscope (OM) and a JEM-2100 transmission electron microscope (TEM) equipped with Oxford Instruments INCA EDS. The samples for OM were etched in a solution containing 4 mL nitric acid and 96 mL ethanol. TEM foils were mechanically ground down to 150 μm and then twin-jet polished in a solution containing 40 mL perchloric acid and 960 mL ethanol at -10 °C followed by final gentle cleaning on a Gatan 691 Precision Ion Polishing System. The hardness of the alloys was measured using an automated Struers DuraScan-50 micro-hardness machine with 0.1 kg load; 20 measurements were taken under each condition.

3. Results

Fig. 1 shows the XRD spectra obtained from the as-cast Mg-4.2Zn-0.8Y (at.%, alloy I), Mg-4.2Zn-0.8Y-0.5Gd (at.%, alloy II) and Mg-4.2Zn-0.8Y-1Gd (at.%, alloy III) alloys. The matrix in all three alloys is α-Mg (hcp, a = 0.321 nm, c = 0.521 nm). Besides the strong Mg peaks, a few weak peaks can be observed in alloy I, which can be indexed as $MgZn_3Y$ (i.e. H phase, hcp, a = 0.918 nm, c = 0.950 nm) and $Mg_3Zn_3Y_2$ (i.e. W phase, fcc, a = 0.683 nm). After the addition of 0.5 at.% Gd (alloy II), the intensity of the peaks associated with W phase increased while the H phase peak becomes no longer observable. A

weak peak which is consistent with the LPSO phase could be observed in alloy II. When Gd content was increased to 1 at.% (alloy III), the XRD spectrum becomes similar to that from alloy II, i.e. W phase is the main secondary phase.

Fig. 2 shows the optical images obtained from the three as-cast alloys. As shown in Fig. 2a, alloy I without Gd contains two types of secondary phases; one is spot-like and dispersed inside the grains; the other type consists of long precipitates along the grain boundaries. The total area fraction of the secondary phases is estimated to be about 4 %. With the addition of 0.5 at.% Gd, the morphology of the precipitates changes, as shown in Fig. 2b. Some areas in grey contrast can be observed inside the grains and were subsequently identified using TEM as a lamellar LPSO/Mg structure (Fig. 5b). The black irregularly-shaped phase either spreads continuously along the grain boundary or disperses inside the grains. The microstructure of alloy III shown in Fig. 2c is similar to that of alloy II, but the area fraction of the W phase has increased from 12 % to 18 %. The LPSO/Mg phase (based on the fraction of grey area) is estimated to have an area fraction of about 16 % and 19 % in alloys II and III respectively.

The average grain size of the as-cast alloys and the area fraction of secondary phases were measured in five images with the same magnification as Fig. 2 using Image J software and are summarised in Table 1, along with the micro-hardness values. The grain size of alloy I (Fig. 2a) is about 400 μm. After adding 0.5 at.% Gd and 1 at.% Gd, the grain sizes of alloy II and alloy III decrease to about 200 μm and 115 μm, respectively. The micro-hardness of the as-cast alloy I is about 64 Hv. With Gd addition, the hardness of alloys II and III increased to 76 Hv and 85 Hv respectively.

Further microstructural characterization of the as-cast alloys was carried out using TEM. Fig. 3a shows a bright field image obtained from the as-cast alloy I, which indicates a W phase particle and an i-phase particle attached together. It should be noted that the i-phase was occasionally observed in the TEM study of all three as-cast alloys, while no peak associated with i-phase has been observed by XRD, presumably due to its low volume fraction. Fig. 3b-d show the composite diffraction patterns obtained from W phase

and i-phase along different zone axes. Fig. 3b was obtained with the electron beam direction close to the [111] zone axis of the W phase which is also close to an axis of 2-fold symmetry of the i-phase. The individual diffraction patterns from i-phase and W phase are shown on the right side. Fig. 3c and 3d are diffraction patterns obtained along the [101] and $[1\bar{1}1]$ zone axes of the W phase which are also parallel to the neighbouring two 2-fold symmetry axes of the i-phase. If the misorientation angle between, for example, the [111] zone axis of the W phase and the 2-fold rotation axis of the i-phase is described as $< [111]_W$, 2-fold$_i$ >, then $< [111]_W$, 2-fold$_i$ >, $< [101]_W$, 2-fold$_i$ > and $<[1\bar{1}1]_W$, 2-fold$_i$ > measured by TEM are 1.2°, 0° and 1.2° respectively. This orientation relationship observed between the i-phase and the W phase is consistent with the literature [10, 22], and has also been observed in the as-cast alloy III, where the [111], [101] and $[1\bar{1}1]$ zone axes of the W phase coincide with the 2-fold, 5-fold and 3-fold rotation axes of the i-phase, where the misorientation angles $< [111]_W$, 2-fold$_i$ >, $< [101]_W$, 5-fold$_i$ > and $< [1\bar{1}1]_W$, 3-fold$_i$ > measured by TEM are 1.9°, 0° and 1.5°. Besides W phase and i-phase, H phase also existed in alloy I (Fig. 4). The diffraction pattern shows the $[0\bar{1}11]$ zone axis of the H phase, which has a hexagonal structure with lattice parameters a = 0.918 nm and c = 0.95 nm.

Typical particles observed in the as-cast alloy II, with 0.5 at. % Gd, are shown in Fig. 5. Fig. 5a shows a bright-field image with W phase lying preferentially at the grain boundaries. The image was taken with the electron beam direction parallel to the [011] zone axis of the W phase (as shown in the insert). Fig. 5b is a bright-field image showing fine LPSO phase lamellae alternating with the Mg matrix. The LPSO phase, appearing dark in the bright-field image, lies parallel to the basal plane of the Mg matrix, as shown by the white arrow indicating the [0001] direction of the Mg matrix. The associated diffraction pattern of the LPSO phase is shown in Fig. 5c and the electron beam direction is parallel to the $[2\bar{1}\bar{1}0]$ zone axis of the Mg matrix. The diffraction pattern of the LPSO phase shows that there are 14 reflections at equal intervals between the transmitted beam and the 0002 reflection spot of pure Mg (included), consistent with the hexagonal 14H structure with lattice parameters a = 0.321 nm and c = 3.694 nm [23].

The chemical compositions of the Mg matrix and the secondary phases were measured using EDS on the TEM and the average values from 10 measurements are listed in Table 2. Shahzad and Wagner [24] have reported that the Zn concentration in the matrix may vary between different regions in a Mg-Zn-Zr alloy. A similar phenomenon has been observed in the current study. In alloy I, the matrix near the grain boundary (about 1 μm away) has a composition of $Mg_{98.28\pm0.11}Zn_{1.59\pm0.12}Y_{0.13\pm0.03}$ at.% while the centre of the grain has a composition of $Mg_{98.89\pm0.31}Zn_{1.06\pm0.31}Y_{0.06\pm0.01}$ at.%, thus the Zn and Y concentrations in the matrix are slightly higher near the grain boundary than at the grain centre. The compositions of the matrix shown in Table 2 were taken from the centres of the grains in the three alloys. In the matrix, the Mg content is 97.5 at.% or above, which means that the solid solution content is less than 2.5 at.%. Before Gd was added, only 0.06 at.% Y was found in the matrix. Y and Gd remained at a low level in the as-cast alloy II when 0.5 at.% Gd was added, but an obvious increase in the Y and Gd concentration in the matrix was observed in alloy III when 1 at.% Gd was added. On the other hand, the Zn concentration shows a different trend from Gd: it increased first to 2.32 at.% in alloy II and dropped to 1.33 at.% in alloy III. In the W phase and i-phase, the total rare earth element (Y and Gd) concentration remained almost unchanged when Gd was added.

4. Discussion

Y and Gd are RE elements and have some similar properties in Mg alloys: 1) the atomic radii of Y and Gd are 0.177 and 0.180 nm, respectively, which are about 11% larger than that of Mg [25]; 2) the electronic configurations of Y and Gd in the ground state are $5d^16s^2$ and $4f^75d^16s^2$ respectively. Both show typical R^{3+} ionic species and contain 3 electrons in the (5d+6s) orbitals (trivalent state) for the metallic state [25]; 3) the solid solubility limits of Y and Gd in Mg are about the same with a value of 1.66 at.% at 372℃ [25]; 4) the diffusion coefficients of Y and Gd in solid Mg are similar, e.g. about 3.5×10^{-15} m^2/s at 470 ℃, which is about one order of magnitude lower than the diffusion coefficients of Al and Zn in Mg [26]. However, different behaviours of Y and Gd were reported in terms of forming

LPSO phases: LPSO phase is observed in the as-cast condition in Mg-1Zn-2Y at.%, but formed only after heat treatment (400 ℃ for 10 h) in Mg-1Zn-2Gd at.% [19, 23]. In this report, the partitioning of Y and Gd between different phases of the three alloys has been analysed. Fig. 6 shows the variation of the Y/(Y+Gd) ratio in different phases with the total Y/(Y+Gd) ratio of the system. The overall Y/(Y+Gd) ratios in alloys I, II, and III are 1, 0.61 and 0.44, respectively. The measured Y/(Y+Gd) ratios from different phases were plotted against the overall Y/(Y+Gd) ratio in the alloys. It is interesting to note that most of the data points can be fitted linearly with a slope close to 1, except for a slight deviation of the data from the W phase in alloy I, and the Mg matrix and the i-phase in alloy II. This indicates that the distribution of Y and Gd in the present phases remains similar and provides the evidence that Gd and Y atoms are interchangeable.

Mg-Zn-Y ternary phase diagrams have been studied with increasing interest due to their good creep resistance at elevated temperature. Padezhnova et al. [27] reported the existence of LPSO phase in the Mg corner of the Mg-Zn-Y phase diagram and Tsai et al. [28] reported the co-existence of liquid, i-phase, W phase and H phase at 427-600 ℃ in the Zn-rich corner. I-phase was reported to be the main secondary phase in an as-cast Mg-4.2Zn-0.8Y at.% alloy [29]. In this work, there were however more W phase and H phase than i-phase which was observed only in a small quantities in alloy I. The co-existence of i-phase and W phase with a specific orientation relationship was also observed in the current study (c.f. Fig. 3a), suggesting that phase transformation from i-phase to W-phase or, *vice versa*, may have occurred during casting. Singh et al [22, 30, 31] reported that the i-phase can transform into H phase upon annealing at 460 ℃, or transform reversibly to W phase at the slightly lower temperature of 448 ℃. An invariant four-phase reaction described as L + W = (Mg) + I at 520 ℃ is also confirmed by Gröbner et al. [11], where detailed Mg-Zn-Y phase diagrams were calculated. Similarly, the reaction L + H = W + I at 526 ℃ also exists [11]. The cooling rate plays a key role during these phase transformations and fast cooling would be expected to suppress this reaction. It is therefore likely that the larger amount of W and H phases

observed in the present work as compared with those reported in the literature may be caused by the modest cooling rate.

In the Mg-Zn-Y-Gd quaternary system, Gd replaces some Y in both the matrix and the secondary phases, thus the quaternary alloy can be simplified to the Mg-Zn-(Y+Gd) ternary system. Upon 0.5 at.% Gd addition, a significant microstructure change has been observed. Lamellar LPSO phase formed in the grain interiors along with more W phase particles and a small amount of i-phase. The secondary phases in Mg-Zn-Y (or Gd) alloys are sensitive to the Zn/Y (or Zn/Gd) ratio [9, 18, 32]. In the Mg-Zn-Y ternary system, Lee et al. [9] reported that i-phase and W phase are the secondary phases when the Zn/Y ratio is between 1.8 to 6 in the Mg-Zn-Y system. When the Zn/Y ratio is between 0.3 and 1, the LPSO phase exists widely [5, 33-36]. Gröbner et al. [11] examined Mg-Y-Zn ternary samples after DSC heating to 900 ℃ and slow cooling at a maximum rate of 5 $K \cdot min^{-1}$; the LPSO phase was observed in the samples when the Zn/Y ratio was 1.2 or 1 and it was absent when the Zn/Y ratio was 2.3 or 4. Meanwhile, Qi et al. [37] calculated the Mg-Zn-Gd ternary phase diagram at 400 ℃ and show that in the Mg-rich corner, with decreasing Zn/Gd ratio, i-phase, W phase, LPSO phase, and Mg_5Gd phase form in sequence. LPSO and W phase co-exist when the Zn/Gd ratio is between 0.75 and 2.22, and the LPSO phase disappears when the Zn/Gd ratio is larger than 2.22, while the W phase disappears when the Zn/Y ratio is smaller than 0.75. The Zn/(Y+Gd) ratios in alloys II and III of the present work are 2.33 and 3.23, respectively. Hence no LPSO phase would be expected, according to the literature. The fact that the LPSO phase was indeed observed in this work when the Zn/(Y+Gd) ratios were 2.33 and 3.23 suggests that Gd addition to Mg-4.2Zn-0.8Y (at.%) may promote the formation of LPSO phase.

With Gd addition, an increase in the microhardness of the alloys was observed. This is probably due to the overall amount of the alloying elements increasing, which would result in a decrease in grain size and an increase in volume fraction of the secondary phases (mainly LPSO and W phase), thus strengthening the alloy via the Hall-Petch relationship and by precipitation hardening. It is worth mentioning that unlike

the hard intermetallic W phase, the LPSO phase is likely to deform by kinking which will introduce lots of kink boundaries and work harden the alloy as a result of refinement [38].

5. Summary

The current study shows that in the Gd-free Mg-4.2Zn-0.8Y at.% alloy, W phase and H phase are the main secondary phases. Upon Gd addition, LPSO phase appears, while W phase remains. LPSO phase exists when the Zn/(Gd+Y) ratios of the alloys are 2.33 and 3.23. The addition of Gd increases the total amount of alloying element and results in a higher amount of secondary phases and smaller grain size which consequently increase the hardness of the as-cast alloys. The EDS results shows no clear differences between the Y and Gd concentration in the various matrices and secondary phases.

Acknowledgement

The authors would like to thank Dr Yu Lu for the help with the sample preparation. JW is grateful for a Li Siguang PhD Scholarship jointly funded by University of Birmingham and the China Scholarship Council.

References

[1] D.H. Bae, M.H. Lee, K.T. Kim, W.T. Kim, D.H. Kim, J. Alloys Compd. 342 (2002) 445-450.

[2] E. Mora, G. Garcés, E. Oñorbe, P. Pérez, P. Adeva, Scripta Mater. 60 (2009) 776-779.

[3] H. Asgharzadeh, E.Y. Yoon, H.J. Chae, T.S. Kim, J.W. Lee, H.S. Kim, J. Alloys Compd. 586 (2014) S95-S100.

[4] T.Y. Kwak, H.K. Lim, S.H. Han, W.J. Kim, Scripta Mater. 103 (2015) 49-52.

[5] Y. Kawamura, K. Hayashi, A. Inoue, T. Masumoto, Mater. Trans. 42 (2001) 1172-1176.

[6] G. Garces, M.A. Muñoz-Morris, D.G. Morris, P. Perez, P. Adeva, Mater. Sci. Eng. A 614 (2014) 96-105.

[7] K. Hagihara, A. Kinoshita, Y. Sugino, M. Yamasaki, Y. Kawamura, H.Y. Yasuda, Y. Umakoshi, Acta Mater. 58 (2010) 6282-6293.

[8] T. Itoi, T. Inazawa, M. Yamasaki, Y. Kawamura, M. Hirohashi, Mater. Sci. Eng. A 560 (2013) 216-223.

[9] J.Y. Lee, D.H. Kim, H.K. Lim, D.H. Kim, Mater. Lett. 59 (2005) 3801-3805.

[10] J.F. Liu, Z.Q. Yang, H.Q. Ye, J. Alloys Compd. 650 (2015) 65-69.

[11] J. Gröbner, A. Kozlov, X.Y. Fang, J. Geng, J.F. Nie, R. Schmid-Fetzer, Acta Mater. 60 (2012) 5948-5962.

[12] K. Kishida, K. Nagai, A. Matsumoto, A. Yasuhara, H. Inui, Acta Mater. 99 (2015) 228-239.

[13] S. Minamoto, T. Horiuchi, S. Miura, Mater. Trans. 56 (2015) 1670-1674.

[14] Y.M. Zhu, A.J. Morton, J.F. Nie, Acta Mater. 58 (2010) 2936-2947.

[15] Z. Zhu, A.D. Pelton, J. Alloys Compd. 652 (2015) 426-443.

[16] J. Gröbner, A. Kozlov, X.-Y. Fang, S. Zhu, J.-F. Nie, M.A. Gibson, R. Schmid-Fetzer, Acta Mater. 90 (2015) 400-416.

[17] H. Somekawa, A. Singh, Y. Osawa, T. Mukai, Mater. Trans. 49 (2008) 1947-1952.

[18] Y. Kawamura, M. Yamasaki, Mater. Trans. 48 (2007) 2986-2992.

[19] M. Yamasaki, M. Sasaki, M. Nishijima, K. Hiraga, Y. Kawamura, Acta Mater. 55 (2007) 6798-6805.

[20] Y. Yang, K. Zhang, M.-L. Ma, J.-W. Yuan, Rare Met. 34 (2015) 160-163.

[21] F. Shi, C.-q. Wang, Z.-m. Zhang, Trans. Nonferrous Met. Soc. China 25 (2015) 2172-2180.

[22] A. Singh, A.P. Tsai, Scripta Mater. 49 (2003) 143-148.

[23] T. Itoi, T. Seimiya, Y. Kawamura, M. Hirohashi, Scripta Mater. 51 (2004) 107-111.

[24] M. Shahzad, L. Wagner, Scripta Mater. 60 (2009) 536-538.

[25] R. Ferro, A. Saccone, S. Delfino, Metall. Sci. Tech. 16 (1998) 25-44.

[26] S.K. Das, Y.-B. Kang, T. Ha, I.-H. Jung, Acta Mater. 71 (2014) 164-175.

[27] E.M. Padezhnova, R.A. Miliyevskiy, T.V. Dobatkina and V.V. Kinshibalo, Russ. Metall. 4 (1982) 185-188.

[28] A.-P. Tsai, Y. Murakami, A. Niikura, Phil. Mag. A 80 (2000) 1043-1054.

[29] A. Singh, M. Nakamura, M. Wantanabe, A. Kato, A.P. Tsai, Scripta Mater. 49 (2003) 417-422.

[30] A. Singh, M. Watanabe, A. Kato, A.P. Tsai, Scripta Mater. 51 (2004) 955-960.

[31] A. Singh, M. Watanabe, A. Kato, A.P. Tsai, Mater. Sci. Eng. A 397 (2005) 22-34.

[32] E. Abe, Y. Kawamura, K. Hayashi, A. Inoue, Acta Mater. 50 (2002) 3845-3857.

[33] M. Noda, T. Mayama, Y. Kawamura, Mater. Trans. 50 (2009) 2526-2531.

[34] K. Hagihara, A. Kinoshita, Y. Sugino, M. Yamasaki, Y. Kawamura, H.Y. Yasuda, Y. Umakoshi, Intermetallics 18 (2010) 1079-1085.

[35] K. Hagihara, N. Yokotani, Y. Umakoshi, Intermetallics 18 (2010) 267-276.

[36] R. Matsumoto, M. Otsu, M. Yamasaki, T. Mayama, H. Utsunomiya, Y. Kawamura, Mater. Sci. Eng. A 548 (2012) 75-82.

[37] H.Y. Qi, G.X. Huang, H. Bo, G.L. Xu, L.B. Liu, Z.P. Jin, J. Mater. Sci. 47 (2012) 1319-1330.

[38] X.H. Shao, Z.Q. Yang, X.L. Ma, Acta Mater. 58 (2010) 4760-4771.

Figure captions:

Fig. 1 XRD spectra obtained from the as-cast alloys.

Fig. 2 Optical micrographs obtained from as-cast alloys: (a) Alloy I contains W phase and H phase; (b) Alloy II with W phase and lamellar LPSO phase; (c) Alloy III with similar microstructure to Alloy II.

Fig. 3 (a) Bright field image obtained from the as-cast alloy I showing a W phase particle joined to an i-phase particle, (b-d) composite diffraction patterns obtained from the i-phase and the W phase shown in (a). Separate diffraction patterns from each of the W phase and i-phase are shown and are indexed on the right side of each composite diffraction pattern: (b) electron beam is parallel to $[111]_{W\ phase}$ and close to a $2\text{-fold}_{i\text{-}phase}$ zone axis; (c) electron beam is parallel to $[101]_{W\ phase}$ and a $2\text{-fold}_{i\text{-}phase}$ zone axis; (d) electron beam is parallel to $[1\bar{1}1]_{W\ phase}$ and close to a $2\text{-fold}_{i\text{-}phase}$ zone axis.

Fig. 4 (a) TEM image of H phase in alloy I; (b) diffraction pattern of H phase; $[0\bar{1}11]$ zone axis.

Fig. 5 (a) Bright-field image and corresponding SAED pattern (inset) of W phase in as-cast alloy II. The electron beam direction is parallel to the [011] zone axis of the W phase; (b) Bright-field image showing the lamellar LPSO phase. The basal plane of the LPSO phase is parallel to that of the magnesium matrix; (c) SAED pattern from centre of (b) confirming that the LPSO phase is of 14H type; the beam direction is parallel to $[2\bar{1}\bar{1}0]$ of the Mg matrix.

Fig. 6 The Y/(Y+Gd) ratios (at. %) measured in different phases versus the overall Y/(Y+Gd) ratios in the three alloys.

Table captions:

Table 1 Grain sizes, area fractions of precipitates and hardness of the three alloys.

Table 2 Compositions of different phases in the as-cast alloys (at.%).

Table 1

	Grain size, μm	**Main precipitates**	**Area fraction, %**		**Hardness, Hv**
			H and W	LPSO/Mg	
Alloy I	400±100	H phase, W phase	4±1	-	64±4
Alloy II	200±55	W phase, LPSO	12±1	16±2	76±6
Alloy III	115±25	W phase, LPSO	18±2	19±2	85±5

Table 2

Phases	**Alloys**	**Element concentration in the phases**			
		Mg	Zn	Y	Gd
Mg matrix	Alloy I	98.89±0.31	1.06±0.31	0.06±0.01	-
	Alloy II	97.48±0.43	2.32±0.42	0.14±0.04	0.06±0.02
	Alloy III	97.73±0.84	1.33±0.63	0.42±0.11	0.53±0.13
W phase	Alloy I	27.53±2.06	44.73±3.50	27.73±4.34	-
	Alloy II	32.84±3.97	41.94±2.50	15.24±1.26	9.98±0.59
	Alloy III	39.79±3.91	34.96±1.50	9.09±1.10	16.16±1.62
i-phase	Alloy I	30.01±1.26	58.52±1.57	11.49±0.62	-
	Alloy II	26.23±0.98	62.67±0.86	5.79±0.19	5.32±0.07
LPSO phase	Alloy III	86.86±1.35	6.97±1.13	2.73±0.23	3.44±0.43

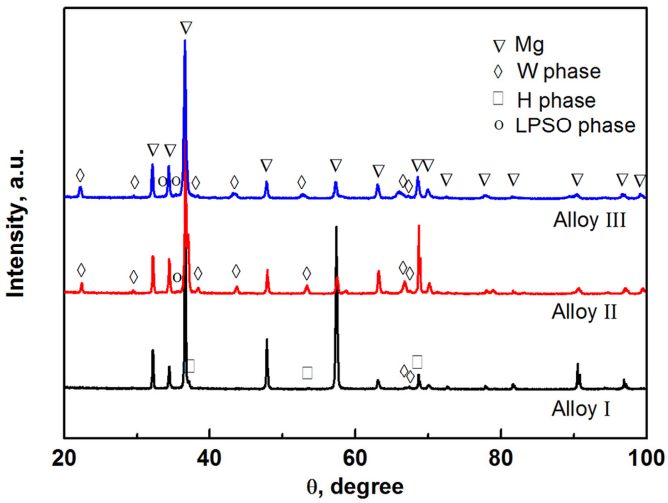

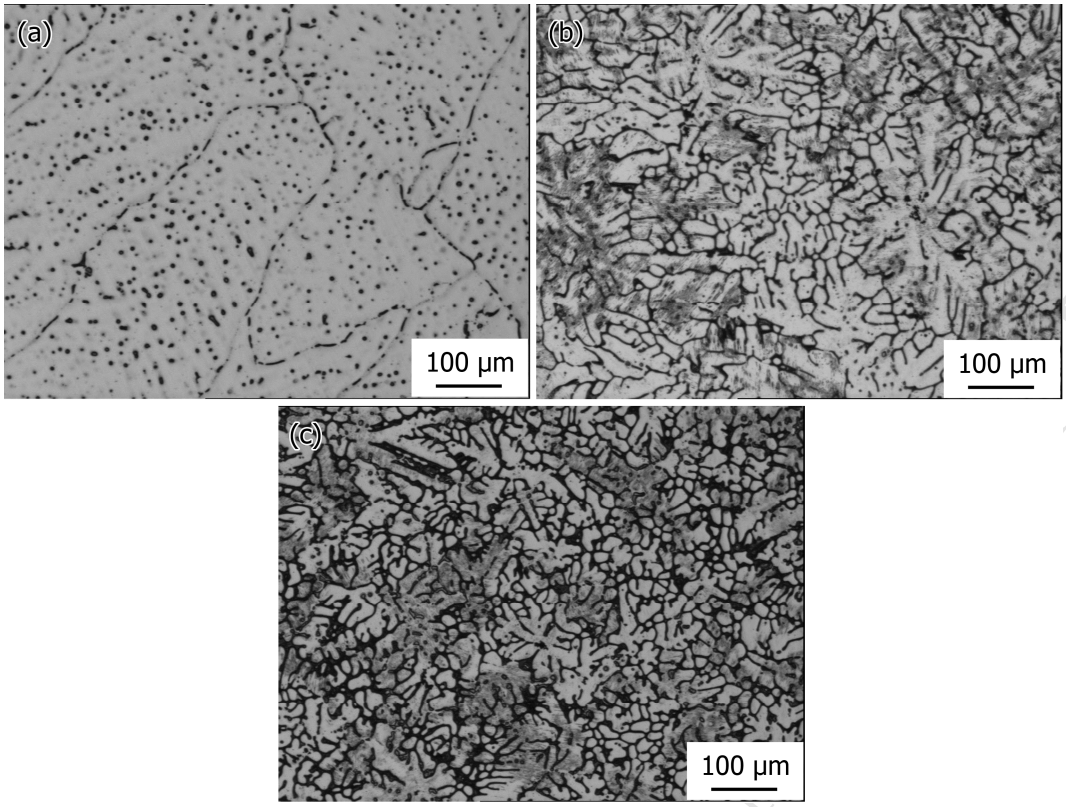

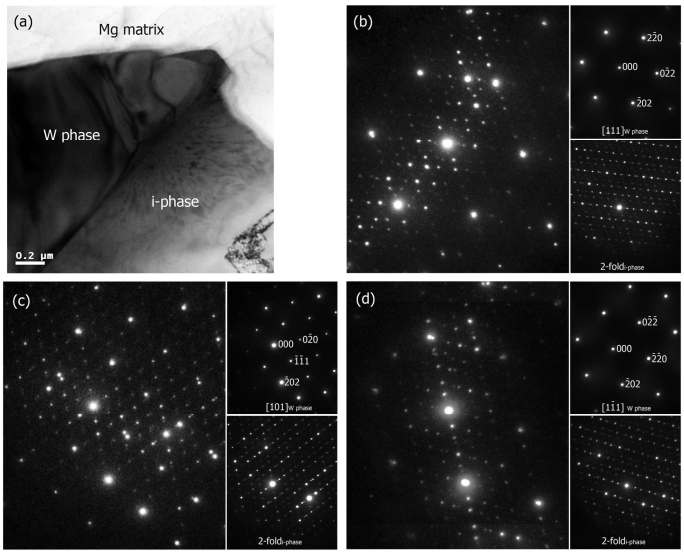

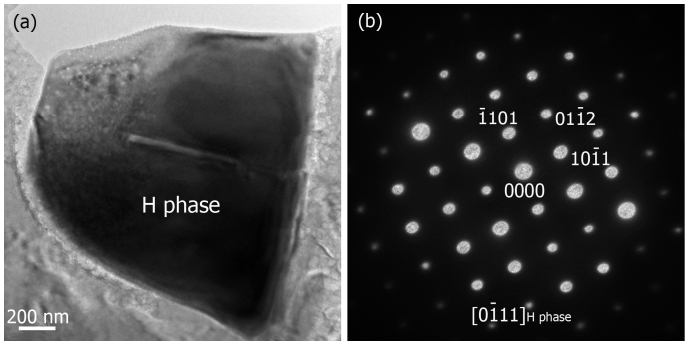

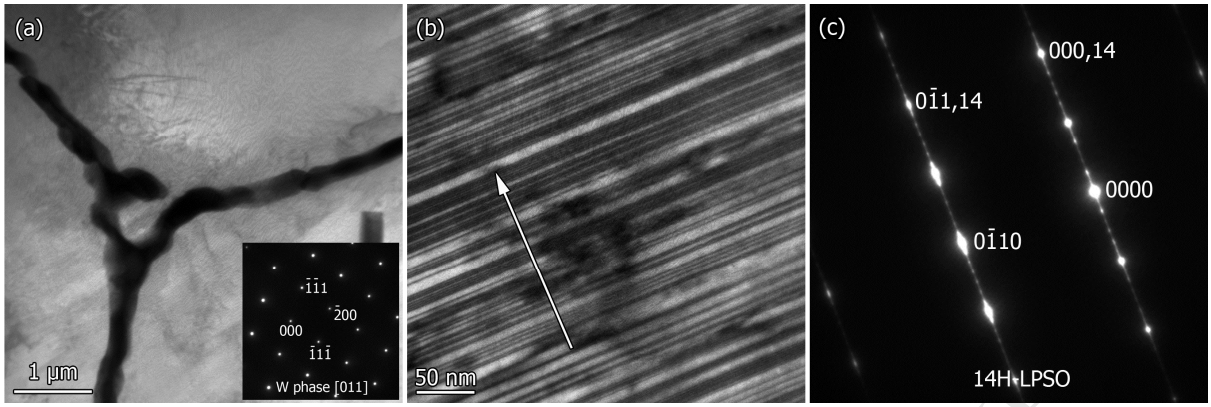

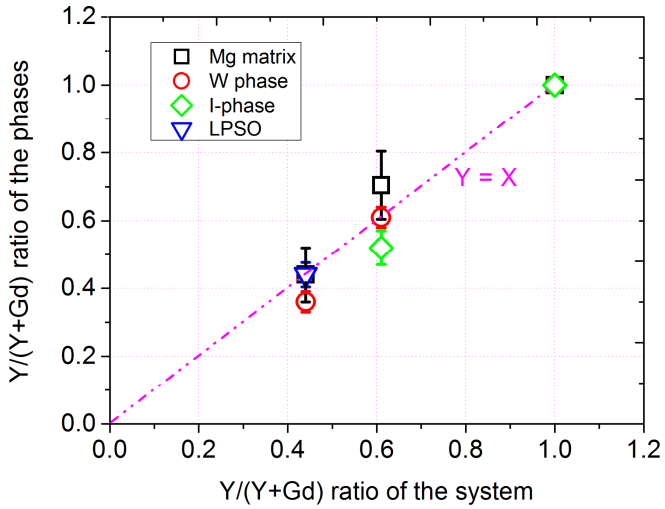

Highlights:

1. The microstructure and hardness of as-cast Mg-Zn-Y-(Gd) alloys were examined.
2. LPSO phase formed after 0.5% Gd addition.
3. The effect of Zn/(Gd+Y) ratio on the secondary phases formation was discussed.
4. No clear preference between Y and Gd partitioning in second phases was observed.